Plant Physiology and Biochemistry 233 (2026) 111264

Contents lists available at ScienceDirect

Plant Physiology and Biochemistry

journal homepage: www.elsevier.com/locate/plaphy

# Tolerance mechanisms to UV-B in olive pollen demonstrate cultivar-dependent biochemical responses

Aslıhan Çetinbaş Genç [a], Silvia Licata [b,1], Giampiero Cai [b,*], Sara Parri [b]

[a] Department of Biology, Faculty of Science, Marmara University, Istanbul, 34722, Türkiye
[b] Department of Life Sciences, University of Siena, via Mattioli 4, Siena, 53100, Italy

ARTICLE INFO

*Keywords:*
Antioxidants
*Olea europaea*
Pollen tube
Reactive oxygen species
Stress-related proteins
Aquaporins
Ultraviolet-B radiation

ABSTRACT

Ultraviolet-B radiation is a major abiotic stress factor that can impair pollen performance and limit plant reproductive success. It primarily targets the architecture of pollen tube cell walls and induces cultivar-specific sensitivity patterns. However, the way in which these structural effects are coordinated with biochemical and molecular responses remains unclear. We examined the responses of pollen grains from three Italian olive cultivars to ultraviolet-B radiation by integrating analyses of reactive oxygen species dynamics, antioxidant capacity and stress-related proteins. Different tolerance strategies were observed among the cultivars. The 'Leccino' cultivar maintained a redox balance through enhanced antioxidant capacity but showed alterations in cytoskeletal and membrane-associated proteins that were likely to affect turgor and pollen tube growth. The 'Olivastra Seggianese' cultivar exhibited a coordinated tolerance strategy involving stable regulation of reactive oxygen species, high levels of polyphenols, sustained induction of heat shock protein 70, and preserved aquaporin and actin, which support tube elongation. By contrast, the 'Pendolino' cultivar exhibited increased levels of reactive oxygen species and significant variability in metabolic and structural parameters, suggesting poor integration of stress responses. Taken together with previous cell wall analyses, these findings show that the ability of olive pollen to tolerate ultraviolet-B radiation depends on the cultivar and is not solely due to individual defensive components, but rather to the coordinated regulation of biochemical, molecular and structural mechanisms.

## 1. Introduction

Solar ultraviolet-B (UV-B) radiation is a major environmental stress factor that affects plant growth, development, and reproduction by inducing DNA damage, protein denaturation, lipid peroxidation, and oxidative stress (Shahzaidi et al., 2025; Mahdavian, 2024). These effects compromise membrane integrity and cellular homeostasis, ultimately reducing plant fitness. While most research has focused on vegetative tissues, the impact of UV-B on generative structures has received far less attention (Zhang et al., 2020; Çetinbaş-Genç et al., 2024). Among these structures, pollen grains are particularly sensitive to UV-B due to their short lifespan, high metabolic activity, and direct exposure to environmental conditions (Kravets et al., 2023).

For species of high economic importance, such as the olive tree (*Olea europaea* L.), which naturally grow under intense solar (UV-B) radiation, pollen performance and response to abiotic stresses is critical for reproductive success and fruit yield (Khaerani et al., 2025). UV-B exposure has been shown to impair pollen viability, germination, and pollen tube elongation in many plant species (Cun et al., 2024; Khaerani et al., 2025). These parameters (viability, germination rate, and tube growth) are widely recognized as consistent indicators of pollen response to abiotic stress (Zhao et al., 2025; Chebli and Geitmann, 2007). Of the many stress targets in the pollen tube, the cell wall is one of the most important, as it contributes to defining the cell shape, and therefore the pollen tube function (Hepler et al., 2013). Previous studies have also highlighted the importance of the pollen tube cell wall as a primary target of environmental stresses, including UV-B (Wang et al., 2016; Parrotta et al., 2016; Cascallares et al., 2020; Çetinbaş-Genç et al., 2024).

In a recent study, we analyzed four Italian olive cultivars ('Frantoio',

* Corresponding author.
*E-mail addresses:* aslihan.cetinbas@marmara.edu.tr (A. Çetinbaş Genç), silvia.licata@unifi.it (S. Licata), cai@unisi.it (G. Cai), sara.parri2@unisi.it (S. Parri).
[1] present address: Dipartimento di Scienze e Tecnologie Agrarie, Alimentari, Ambientali e Forestali, University of Florence, Piazzale Delle Cascine 18, 50144 Florence, Italy.

https://doi.org/10.1016/j.plaphy.2026.111264
Received 23 December 2025; Received in revised form 21 March 2026; Accepted 31 March 2026
Available online 2 April 2026

'Leccino', 'Olivastra Seggianese', and 'Pendolino') to assess the effects of UV-B radiation on pollen grains and tubes. We evaluated pollen viability, germination rate, pollen tube length, and the distribution of cell wall components; we found that the pollen tube cell wall likely represents the primary target or defense mechanism against UV-B stress (Çetinbaş-Genç et al., 2024). In addition, the manuscript demonstrated that each cultivar's pollen exhibited a distinct sensitivity profile to UV-B radiation. These responses were dependent on both intensity and duration of exposure; frequent exposure typically reduced viability and growth, whereas prolonged, low-intensity exposure yields variable effects. Analyses of pollen cell walls revealed alterations in the distribution of pectins, cellulose, callose, CalS, and AGP, accompanied by swelling and loss of polarity. Cultivar sensitivity differed significantly: 'Frantoio' and 'Leccino' exhibited greater sensitivity to high intensities, 'Pendolino' was susceptible to prolonged low intensities, and 'Olivastra Seggianese' demonstrated intermediate tolerance. These results suggested that pollen resilience to UV-B is related to the preservation of apical growth and cell wall integrity. However, it remains unclear whether the cell wall is the sole (direct or indirect) compartment affected or whether UV-B triggers broader biochemical changes. UV-B is known to induce excessive reactive oxygen species (ROS) production (Cun et al., 2024), which can compromise membrane structure and cell wall integrity (Khaerani et al., 2025; Sharma et al., 2017). As the pollen tube is a highly polarized and dynamic structure whose growth depends on a balance between ROS signaling and antioxidant defenses, enzymatic antioxidants such as superoxide dismutase (SOD) and catalase (CAT) play a central role in maintaining redox homeostasis during tip growth. The concerted regulation of SOD and CAT, in addition to total phenolic and flavonoid compounds, is essential for maintaining the redox homeostasis necessary for polarized pollen tube growth (Fujita and Hasanuzzaman, 2022; Martin et al., 2022). SOD converts superoxide radicals primarily produced by plasma membrane NADPH oxidases (RBOHs) into $H_2O_2$ (Martin et al., 2022; Potocký et al., 2007). The localized accumulation of $H_2O_2$ is essential for sustaining elongation and correlates with the rapid influx of calcium that drives tip growth (Kaya et al., 2014). CAT is mainly found in peroxisomes and breaks down $H_2O_2$ to prevent excessive accumulation (Podolyan et al., 2021), which could lead to depolymerized (balloon-like) growth (Podolyan et al., 2021). This is demonstrated by evidence that up-regulation of SOD significantly improves pollen germination and viability (Podobedova et al., 2025). Precise spatial regulation of these enzymes is therefore essential for pollen tube growth (Xie et al., 2022).

Beyond antioxidant enzymes, reproductive plant tissues also rely on non-enzymatic antioxidants, such as flavonoids and polyphenols (Xie et al., 2022). Flavonoids act as antioxidants against UV-B radiation and regulate cellular signaling (Shi and Liu, 2021; Ulm and Jenkins, 2015); flavonols are a key subgroup that is required for male fertility in several plant species (Muhlemann et al., 2018). Pollen mutants that are deficient in flavonol synthesis have higher levels of ROS and are more sensitive to heat stress (Muhlemann et al., 2018). Other non-enzymatic defenses include polyamines such as spermidine, which regulate the redox status and boost the activity of antioxidant enzymes (Xie et al., 2022; Podolyan et al., 2021).

Other proteins also contribute to stress adaptation in pollen tubes. HSPs, particularly HSP70, prevent protein denaturation and facilitate protein refolding under abiotic stress conditions (Ren et al., 2019; Mukhopadhyay et al., 2024). They are widely used to monitor stress responses in plant cells, including pollen (Pan et al., 2024). Exposure to UV-B radiation has been shown to alter HSP70 levels in pollen tubes (Del Casino et al., 2024). HSP70 is also associated with a pollen tube kinesin (Parrotta et al., 2013) suggesting that changes in its activity could affect the slow movement of organelles and vesicles along microtubules. Cytoskeletal components, including actin filaments and microtubules, are highly responsive to UV-B (Du et al., 2021; Krasylenko et al., 2013). UV-B radiation causes microtubules to reorganize rapidly, resulting in randomization and fragmentation, and widespread depolymerization (Krasylenko et al., 2012, 2013). Exposure to UV-B radiation triggers the aggregation of actin filaments, resulting in gathering of actin filaments into bundles (Du et al., 2021; Chen and Han, 2016). This altered actin distribution is associated with a localized burst of ROS (Du et al., 2021). In addition, actin filaments orchestrate a rapid nuclear avoidance movement (Iwabuchi et al., 2016; Du et al., 2021). Moreover, UV-B stress can also result in changes to the cytosolic levels of actin and tubulin (Del Casino et al., 2024). Among the actin filament-associated proteins, sucrose synthase (SuSy) is a key enzyme in plant metabolism that also provides carbon substrates (UDP-glucose) for the synthesis of cellulose and callose (Lei et al., 2012; Salnikov et al., 2001; Winter et al., 1998). SuSy can also store sucrose energy as UDP-glucose, which is useful in stressful situations. The dual role of SuSy depends on its localization: either in the cytosol or associated with the cell membrane. The latter depends on SuSy interaction with actin filaments (Persia et al., 2008). While the impact of UV-B radiation on SuSy levels remains unclear, it is known that UV stress affects the periodicity of callose plug deposition, potentially impacting turgor pressure (Del Casino et al., 2024). The maintenance of turgor pressure in the pollen tube also depends on the influx of water, which is facilitated by specific proteins, such as aquaporins (AQPs) (Sommer et al., 2008; Perez Di Giorgio et al., 2017). SIP2; 1 is an ER-localized AQP involved in pollen germination and pollen tube elongation in *Arabidopsis thaliana*. Mutants lacking SIP2; 1 exhibited a reduction in pollen germination rates and pollen tube lengths, affecting fertility and reducing seed number in mutant siliques. NIP4; 1 and NIP4; 2 are two pollen-specific AQPs; expression of NIP4; 2 peaks during pollen tube growth and is correlated with enhanced water transport. Reduced germination rates in NIP4 mutants underscore the importance of AQPs in pollen tube emergence and elongation.

Despite the recognized roles of these molecular actors in stress responses, their combined contribution to UV-B tolerance in pollen remains poorly understood. UV-B-induced changes at the cell wall level (Çetinbaş-Genç et al., 2024) appear just as one consequence of UV-B exposure, suggesting that additional tolerance mechanisms are present. Given that previous studies have shown that stress tolerance varies not only among species but also among cultivars (Tan et al., 2023; Piccini et al., 2021; Zeng et al., 2024), we hypothesized that studying cultivar-specific responses would clarify the different biochemical strategies. Therefore, our aim is to identify tolerance mechanisms and establish links between biochemical responses and cell wall alterations that have been observed previously. To this end, we also employed a heatmap approach to visualize correlations among molecular indicators and reveal cultivar-specific patterns. This allows us to move beyond isolated parameter analysis towards a comprehensive understanding of pollen adaptation to UV-B stress.

## 2. Materials and methods

### 2.1. Pollen material

Pollen grains of three Italian olive cultivars (*Olea europaea* L.; 'Leccino', 'Olivastra Seggianese', and 'Pendolino') were collected in May 2025 from rainfed, non-fertilized olive trees older than 10 years growing naturally at the Follonica site (Grosseto, Tuscany, Italy) of the National Research Council of Italy, Institute of BioEconomy. For each cultivar, pollen collected during a single sampling period was pooled and used for all subsequent analyses. The cultivar 'Frantoio', included in the previous study (Çetinbaş-Genç et al., 2024), was not analyzed here due to unavailability of fresh pollen during the sampling period. After collection, pollen samples were dehydrated for 24 h in a silica-gel desiccator at room temperature and stored at −20 °C until use. Prior to experiments, samples were equilibrated for 30 min at 4 °C and then rehydrated overnight at room temperature.

### 2.2. UV-B exposure and in vitro germination of pollen grains

UV-B radiation was provided by a TL20W/12 lamp (Philips, Milan, Italy), which emits radiation in the 'B' bandwidth of the UV spectrum (290 to 315 nm) and has been widely described in the literature (Allen Brady and Halloran, 1997). Based on the cultivar-specific response index established in our previous study (Çetinbaş-Genç et al., 2024), the UV-B treatment groups used in the present work were selected to represent the most and least stressful conditions for each cultivar. UV-B treatments were applied by adjusting both the distance between the lamp and the samples and the exposure duration. The same experimental setup was used as in our previous study (Çetinbaş-Genç et al., 2024). The radiation output of the UV-B lamp was verified using an 840 Power Meter equipped with an 818-UV sensor (Newport Optical, Irvine, CA, USA). Specifically, samples placed at 10 cm from the lamp were exposed to an irradiance of 7 $W/m^2$ (considered acute stress), while samples at 40 cm received 2 $W/m^2$ (a value very similar to the natural irradiance on a sunny summer's day in a mid-latitude region) (Kasthurirengan et al., 2025). The same UV-B lamp, experimental setup and exposure geometry were consistently used throughout all experiments, enabling reliable relative comparisons between treatments. The cumulative stress response index classification was defined by integrating pollen viability, germination rate, and pollen tube elongation responses under varying UV-B intensities and exposure durations. Accordingly, for Leccino and Olivastra Seggianese, the 10 cm/2 h exposure corresponded to the high-stress condition, while 40 cm/2 h (Leccino) and 40 cm/1 h (Olivastra Seggianese) represented the low-stress condition. In Pendolino, 10 cm/3 h and 40 cm/1 h were chosen as high- and low-stress conditions, respectively. Rehydrated pollen grains of each cultivar were exposed to UV-B radiation under the conditions described above and thoroughly described in Çetinbaş-Genç et al. (2024). Pollen grains from the control groups were not subjected to UV-B exposure. Afterwards, pollen grains were germinated for 4 h in Brewbaker & Kwack medium containing 8% sucrose (Brewbaker and Kwack, 1963).

### 2.3. Determination of ROS distribution

To investigate the effects of UV-B radiation on the distribution of ROS in pollen tubes, samples were incubated with 10 μM 5-(and 6-) chloromethyl-2′,7′-dichlorodihydrofluorescein diacetate ($H_2$DCFDA) and subsequently visualized under fluorescence excitation/emission at 530-540 nm (Serrazina et al., 2014). At least three independent preparations were analyzed for each treatment condition. Due to rapid signal decay, images were acquired within 5 min under identical settings and focal conditions. Pseudo color imaging was applied to enhance the visualization of differential ROS concentrations along the pollen tubes. Integrated density (I.D.) was quantified in 30 pollen tubes per treatment along the growth axis (tip to 100 μm) using the ImageJ "Segmented Line" tool with a line width sufficient to cover the pollen tube diameter. After fluorescence profiles were obtained, curve similarities among treatments were evaluated, and $R^2$ values were calculated in RStudio using Pearson correlation analysis to quantify the correspondence between their ROS distribution patterns. Since the comparison was conducted with reference to the control group, the $R^2$ value of the control group was defined as 1, while the $R^2$ values of the treatment groups ranged from 0 to 1. A high $R^2$ value indicated a strong correspondence between the curves, whereas a low $R^2$ value reflected greater divergence among them.

### 2.4. Determination of antioxidant capacity, total polyphenols and flavonoids

To evaluate the effects of UV-B radiation on the antioxidant capacity and the total polyphenol and flavonoid contents, pollen tubes were extracted in 70% acetone. A single extract was prepared for each treatment condition, and all spectrophotometric measurements were performed in triplicate. The total antioxidant capacity was determined using the ferric reducing antioxidant power (FRAP) method (Benzie and Strain, 1996). For each measurement, 204 μL of 300 mM acetate buffer (pH 3.6), 20 μL of 10 mM TPTZ solution (2,4,6-tripyridyl-s-triazine), 20 μL of 20 mM $FeCl_3$, and 2 μL of extract ($dH_2O$ for the blank) were mixed. The reaction mixture was incubated at 37 °C for 1 h, and absorbance was recorded at 593 nm using a microplate reader. Results were calculated against a ferrous sulfate calibration curve and expressed as mmol $Fe^{2+}$ equivalents per 100 g of pollen.

Total polyphenol content was determined using the Folin–Ciocâlteu colorimetric method (Singleton and Rossi, 1965). The reaction mixture was prepared by adding 25 μL of extract ($dH_2O$ for the blank), 197.5 μL of distilled water, 12.5 μL of Folin–Ciocâlteu reagent, and 37.5 μL of saturated sodium carbonate ($Na_2CO_3$) solution. The mixtures were incubated at 37 °C for 30 min, and absorbance was measured at 795 nm using a microplate reader. Total polyphenol concentration was calculated from a gallic acid standard curve and expressed as mg gallic acid equivalents (GAE) per 100 g of pollen.

Total flavonoid content was determined using the aluminum chloride colorimetric method (Smirnova and Pervykh, 1998). The reaction mixture was prepared by adding 25 μL of extract ($dH_2O$ for the blank), 75 μL of 95% ethanol, 5 μL of 10% aluminum chloride, 5 μL of 9.8% potassium acetate, and 140 μL of distilled water. The mixtures were incubated at room temperature for 1 h, and absorbance was measured at 415 nm using a microplate reader. Total flavonoid concentration was calculated from a quercetin standard curve and expressed as mg quercetin equivalents (QE) per 100 g of pollen.

### 2.5. Analysis of stress-related proteins

To examine the effects of UV-B radiation on stress-related protein levels in pollen tubes, we performed a differential extraction procedure. Samples were homogenized in HEM buffer containing 1 mM DTT (50 mM HEPES, pH 7.5; 2 mM EGTA; 2 mM $MgCl_2$). The homogenate was centrifuged at 16,000×*g* for 1 h at 4 °C. The resulting supernatant and pellet were used as the cytosolic and membrane fractions, respectively. The cytosolic and membrane protein fractions were treated as independent extracts for subsequent analysis. Each fraction was mixed with Laemmli sample buffer (20% glycerol, 2% SDS, 0.032% bromophenol blue, 2% β-mercaptoethanol, 0.25 M Tris-HCl, pH 6.8), incubated at 90 °C for 5 min, and centrifuged at 16,000×*g* for 2 min. Supernatants were used as the protein sources for subsequent analyses (Del Casino et al., 2024).

Stress-related proteins were analyzed by one-dimensional SDS-PAGE and immunoblotting. The TGX Stain-Free FastCast Acrylamide Kit (Bio-Rad) was used for gel preparation according to the manufacturer's instructions. Gels containing 10% acrylamide were used for CAT, HSP70, tubulin, actin, and SuSy, while 12% gels were used for AQPs and SOD. Electrophoresis was carried out at 200 V for 35-45 min using a 10-250-kDa protein marker and XT MOPS (Bio-Rad Laboratories, Hercules, CA, USA) as the running buffer. Proteins were transferred onto nitrocellulose membranes using a Trans-Blot system (2.5 A, 25 V, 7 min). After blocking in EveryBlot Blocking Buffer (Bio-Rad), membranes were incubated for 1 h with the following primary antibodies: anti-16-kDa Cu/Zn SOD (1:1500, AS184243 Agrisera) (Del Casino et al., 2024), anti-55-kDa CAT (1:1000, AS09501 Agrisera) (Del Casino et al., 2024), anti-75-kDa HSP70 (1:5000, AS081371 Agrisera) (Piccini et al., 2021), anti-50-kDa tubulin (1:3000, Agrisera) (Del Casino et al., 2024), anti-43-kDa actin (1:3000, Agrisera) (Del Casino et al., 2024), anti-80-kDa SuSy1 (1:5000, AS152830 Agrisera) (Persia et al., 2008), and anti-37-kDa AQP (1:1000, Agrisera) (Conti et al., 2022). Secondary antibodies were applied as follows: StarBright Blue 700 nm-conjugated anti-rabbit IgG (1:2500; 12004161 Bio-Rad) for HSP70, SuSy, AQP, SOD, and CAT, and StarBright Blue 520 nm-conjugated anti-mouse IgG (1:2500; Bio-Rad) for actin and tubulin. After antibody incubation, immunoreactive protein bands were visualized and quantified using the

ChemiDoc gel visualizing instrument. Immunoblot signal quantification was performed using Bio-Rad Image Lab software (version 6.1; Bio-Rad, Hercules, CA, USA). Each membrane was visualized in the Stain-Free Blot channel, with the lane displaying the highest protein abundance selected as the reference. This lane was then used to normalise the proteins present in all the other lanes on the same membrane. The intensity of the immunoblotting signal in each lane was then normalized according to the relative protein content. The obtained I.D. values were normalized separately for each cultivar and fraction on a scale from 1 to 100 to facilitate comparison among treatments. Immunoblot analyses were performed using single cytosolic and membrane extracts per treatment condition.

### 2.6. Statistical analysis

Unless otherwise stated, statistical analyses were performed on triplicate technical measurements. Statistical comparisons of measurement results were performed using one-way ANOVA followed by Tukey's HSD post hoc test in the SPSS software ($p < 0.05$) (Koubouris et al., 2009). For the heat-map evaluation, $R^2$ values derived from the ROS analyses were included. In the case of other parameters, the optimal condition of each cultivar was taken as the reference (control) group. To assess the influence of UV-B radiation on these parameters, the percentage change of each variable was calculated relative to its respective control. Because increases or decreases in the measured values could not be directly interpreted as beneficial or detrimental for pollen tube behavior, the absolute values of percentage changes were used when constructing the heat map. To integrate and visualize the parameter variations, a heat map was generated in the R environment (RStudio interface) using the "pheatmap" package. The customized script developed for this study applied a "row" scaling approach. Control groups were excluded from the clustering process; therefore, six experimental groups were analyzed in total. To improve the interpretability of the figure, the dataset was normalized on a scale from 1 to 6, assigning 1 to the lowest and 6 to the highest value in each row. Clustering of both rows and columns was conducted based on Euclidean distance (Galili et al., 2018). Pearson correlation analysis was performed on percentage change values across all treatment groups (n = 6) to quantitatively assess the relationships among the measured biochemical and structural parameters. To highlight patterns that emerged consistently across different cultivars, a correlation analysis was carried out on the combined dataset. Pooling the experimental conditions allowed for a more robust statistical evaluation and made it easier to identify general associations among the measured parameters under UV-B exposure. This approach offered a broader view of UV-B responses in olive pollen. Correlation coefficients (r) were calculated using the Pearson method in the R statistical software package. The statistical significance of the correlations was evaluated using two-tailed tests, with p-values below 0.05 being considered significant. Due to the small number of experimental groups, the correlation results were interpreted as indicative of associations rather than as definitive causal relationships.

## 3. Results

### 3.1. ROS distribution and antioxidant responses

In 'Leccino', ROS distribution showed a similar trend in the control group and after a 2 h exposure at 10 cm, increasing to approximately 6 μm and then gradually decreasing. However, after a 2 h exposure at 40 cm, the ROS signal increased to approximately 6 μm and then stabilized (Fig. 1a). Fig. 1b shows that the control (blue line) and the 10 cm/2 h exposure (red line) exhibited similar trends. The 40 cm/2 h exposure

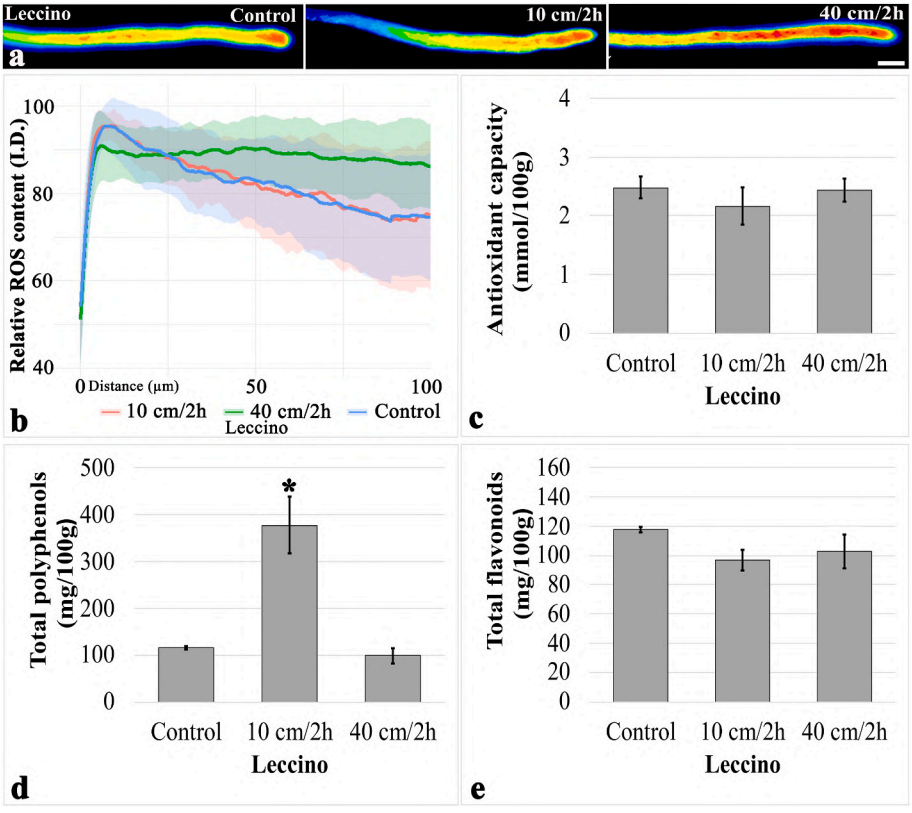


**Fig. 1.** The effect of UV-B radiation on ROS distribution and antioxidant capacity in 'Leccino'. **a** ROS distribution along the pollen tubes under control condition (left panel), at 10 cm/2 h exposure (central panel) and at 40 cm/2 h (right panel); **b** I.D. measurement of ROS starting from the tube apex (100 μm); **c** Antioxidant capacity in the three experimental conditions; **d** Total polyphenol content in the three experimental conditions; **e** Total flavonoid content in the three experimental conditions. Bar: 20 μm. Data represent means ± SD; asterix indicates significant differences ($p < 0.05$).

(green line) showed a distinct divergence from these two samples. Based on the ROS distribution observed in the control sample, which exhibited a peak at the pollen tube tip followed by a consistent decrease along the shank, only the samples treated for 2h at 40 cm showed a different behavior. These samples displayed a uniform ROS content along the entire length of the pollen tube. To quantitatively evaluate the results, we assessed the similarity between the treatment and control curves using $R^2$ values, where higher values indicate greater similarity. The $R^2$ value was 0.97 for the 2 h exposure at 10 cm and 0.32 for the 2 h exposure at 40 cm.

The antioxidant activity of the treated samples remained unchanged compared to the control (Fig. 1c). However, total polyphenol content increased by 227.44% relative to the control after 2 h of UV-B exposure at 10 cm. In contrast, treatment for 2 h at 40 cm did not result in a significant change (Fig. 1d). Total flavonoid content did not significantly differ from the control under either treatment condition (Fig. 1e). Samples with significantly higher polyphenol content exhibited a ROS distribution similar to that of the control. Conversely, samples with substantially different ROS profiles did not show significant increases in polyphenol content.

Similar trends in ROS signal intensity were observed in treated and untreated control samples of 'Olivastra Seggianese' under two different treatment conditions. In both groups, ROS signal intensity increased, peaking at around 10 μm, before decreasing slightly and consistently (Fig. 2a and b). The $R^2$ values, which are used to quantify the goodness of fit, were found to be 0.84 for the 2 h exposure at 10 cm and 0.91 for 1 h exposure at 40 cm. These values indicate a strong correlation between the distance from pollen tube tip and ROS signal intensity. UV-B exposure did not alter ROS distribution in pollen tubes compared to the control. There was no significant difference in antioxidant activity compared to the control under either treatment condition (Fig. 2c). However, exposure to UV-B for 2 h at 10 cm increased the total polyphenol content by 62.80%, whereas exposure for 1 h at 40 cm had no significant effect (Fig. 2d). The total flavonoid content did not change significantly from the control under either treatment condition (Fig. 2e). However, the basal polyphenol content of 'Olivastra Seggianese' is at least twice that of 'Leccino', which suggests an inherent protective activity. This could explain the stable ROS distribution and minor increase in polyphenol content in 'Olivastra Seggianese'.

In the 'Pendolino' experiment, the control group exhibited a significant increase in the ROS signal, peaking at around 6 μm and then declining steadily. Both treatment groups displayed similar ROS responses, with the signal increasing to around 10 μm before stabilizing and remaining relatively constant (Fig. 3a and b). Correlation analysis between treatment and ROS signal yielded an $R^2$ value of 0.06 for the 3 h exposure at 10 cm, indicating a weak positive correlation. 1 h exposure at 40 cm showed an even weaker relationship, with a very low $R^2$ value of 0.03. Following 3 h UV-B exposure at 10 cm, antioxidant activity increased by 42.01% compared to the control. In contrast, 1 h exposure at 40 cm did not result in any significant changes (Fig. 3c). The total polyphenol content remained stable following a 3 h exposure at 10 cm. However, 1 h UV-B exposure at 40 cm resulted in a 70.86% reduction compared to the control (Fig. 3d). Total flavonoid content increased by 32.64% relative to the control after 3 h UV-B exposure at 10 cm; however, 1 h exposure at 40 cm did not induce significant changes (Fig. 3e). The stability of polyphenol levels also indicates significant changes in the ROS distribution profile in the two experimental conditions compared to the control. Previous experimental studies have demonstrated a correlation between variations in the ROS profile and changes in polyphenol content. In this case, however, none of the treated samples exhibited increased polyphenol levels. In fact, the sample exposed to 40 cm for 1 h showed a decrease in polyphenol content. This suggests that

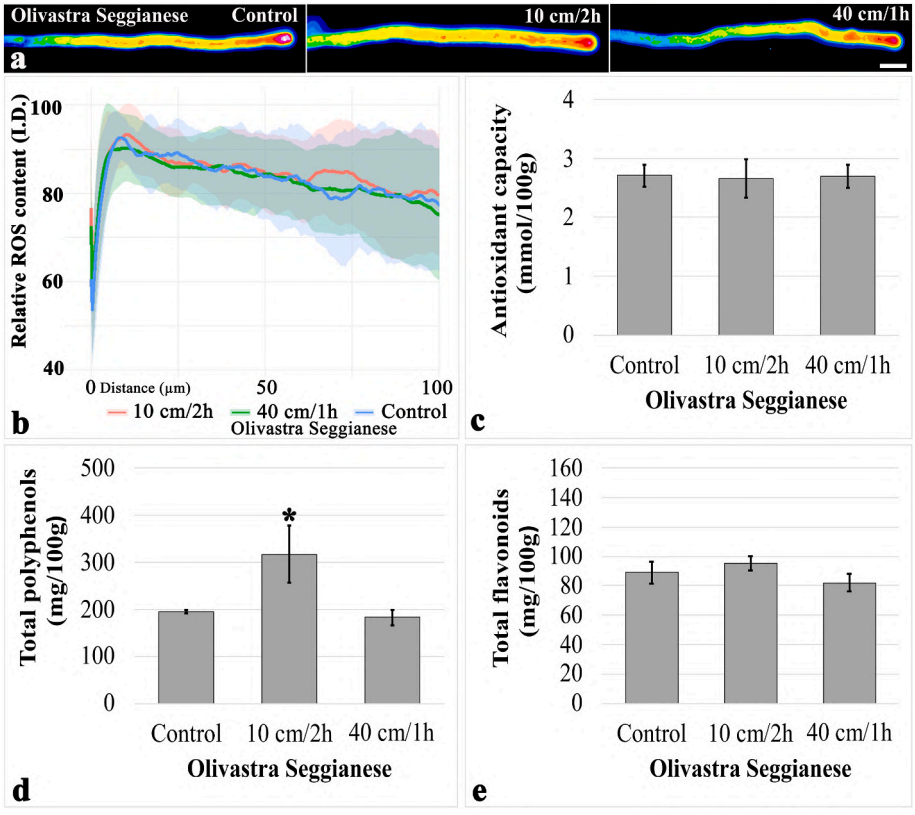


**Fig. 2.** The effect of UV-B radiation on ROS distribution and antioxidant capacity in 'Olivastra Seggianese'. **a** ROS distribution along the pollen tubes for the first 100 μm from the tube apex under control condition (let panel), at 10 cm/2 h exposure (central panel) and at 40 cm/1 h (right panel); **b** I.D. measurement of the ROS signal. **c** Antioxidant capacity under the three experimental conditions. **d** Total polyphenol content under the three experimental conditions. **e** Total flavonoid content under the three experimental conditions. Bar: 20 μm. Data represent means ± SD; asterix indicates significant differences ($p < 0.05$).

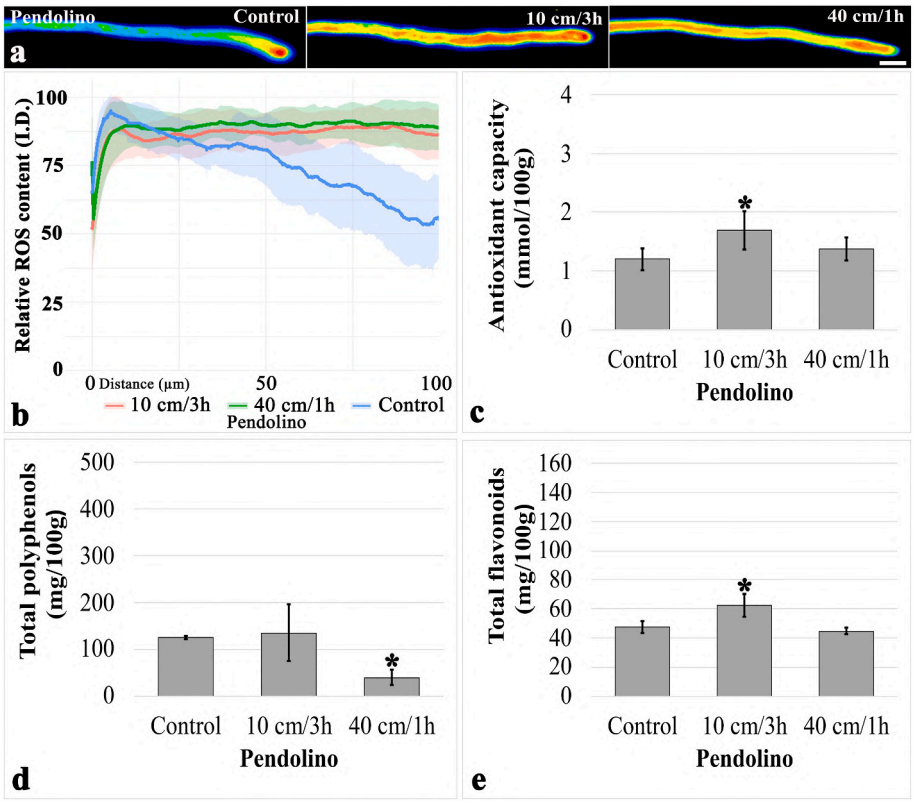


**Fig. 3.** The effect of UV-B radiation on ROS distribution and antioxidant capacity in 'Pendolino'. **a** ROS distribution along the pollen tubes for the first 100 µm of length under control condition (left panel), at 10 cm/3h exposure (central panel) and at 40 cm/1h (right panel); **b** I.D. of the ROS distribution; **c** Antioxidant capacity under the three experimental conditions; **d** Total polyphenol contents under the three experimental conditions; **e** Total flavonoid contents under the three experimental conditions. Bar: 20 µm. Data represent means ± SD; asterix indicates significant differences ($p < 0.05$).

the 'Pendolino' pollen has limited protective capacity against UV exposure. Interestingly, 'Pendolino', like 'Leccino', had half the basal polyphenol content of 'Olivastra Seggianese'.

### 3.2. Stress-related and structural proteins

To provide a more detailed assessment of cellular responses to UV-B radiation at the protein level, we analyzed the levels of stress-related and structural proteins in membrane and cytosolic fractions. These proteins included SOD, CAT, HSP70, SuSy, AQP, actin and tubulin. Immunoblot analyses of 'Leccino' pollen extracts (Fig. 4a) showed the presence of the target proteins in both the membrane and the cytosolic fractions under all experimental conditions. However, their relative abundance differed between the two compartments. The SOD content was lower in the membrane samples than in the cytosolic fraction. The CAT analysis revealed an opposite trend, showing higher levels of protein in the membrane fraction and lower levels in the cytosol. HSP70 was evenly distributed, although slightly more abundant in cytosolic extracts. SuSy was more concentrated in the cytosol, with a weaker signal observed in the membrane fraction. AQP exhibited a distinct profile, with a single 37-kDa band detected in the membrane fraction and two bands (approximately 37 and 50-kDa) observed in the cytosolic samples. Actin was distributed relatively evenly between the membrane and cytosolic fractions, whereas tubulin was more concentrated in the cytosolic samples.

Following both treatments, SOD levels increased in both the membrane and cytosolic fractions (Fig. 4b), suggesting that SOD may function as a defense protein against UV-B exposure. CAT levels in the membrane fraction showed a slight increase under both treatment conditions. In the cytosol, however, CAT levels increased after a 2 h UV-B exposure at 10 cm but decreased after a 2 h UV-B exposure at 40 cm, compared to the control (Fig. 4c). HSP70 levels decreased in membrane fractions after both treatments, while cytosolic HSP70 content remained relatively stable (Fig. 4d). SuSy levels in the membrane fraction increased following 2 h UV-B exposure at 10 cm; however, there was no change compared to the control following a 2 h UV-B exposure at 40 cm. SuSy levels in the cytosolic fraction remained stable across control and treated samples (Fig. 4e). A 37-kDa AQP immunoreactive band was detected in all fractions of the control group and the UV-B-treated group. The 37-kDa AQP content decreased in the membrane fractions of both groups, while the levels of 37-kDa AQP in the cytosolic fraction slightly increased following the 40 cm/1 h exposure. In contrast, 50-kDa AQP was not detected in the membrane fraction but showed a consistent increase in the cytosolic fraction following both treatments (Fig. 4f). In the membrane fraction, actin levels decreased after both treatments, whereas actin levels in the cytosol were similar to the control after a 2 h UV-B exposure at 10 cm, but increased after a 2 h UV-B exposure at 40 cm (Fig. 4g). Finally, tubulin levels in the membrane fraction increased following a 2-h UV-B exposure at 10 cm, but decreased following a 2 h UV-B exposure at 40 cm. The opposite trend was observed in the cytosolic fraction: tubulin levels decreased after a 2 h UV-B exposure at 10 cm and increased after a 2 h UV-B exposure at 40 cm (Fig. 4h).

Compared to the control group, immunoblot analysis of 'Olivastra Seggianese' pollen after UV-B exposure revealed a weak SOD signal associated with the membrane fraction and a variable SOD signal in the cytosolic fraction, where the protein appeared to be more abundant. CAT expression was stronger in the membrane fraction than in the cytosol. HSP70 was distributed more evenly between the two fractions, with a slight prevalence in the latter. SuSy was more abundant in the cytosolic fraction than in the membrane fraction. In contrast to 'Leccino' pollen, 'Olivastra Seggianese' pollen exhibited a single AQP isoform with a molecular weight of around 37-kDa. The distribution of actin was

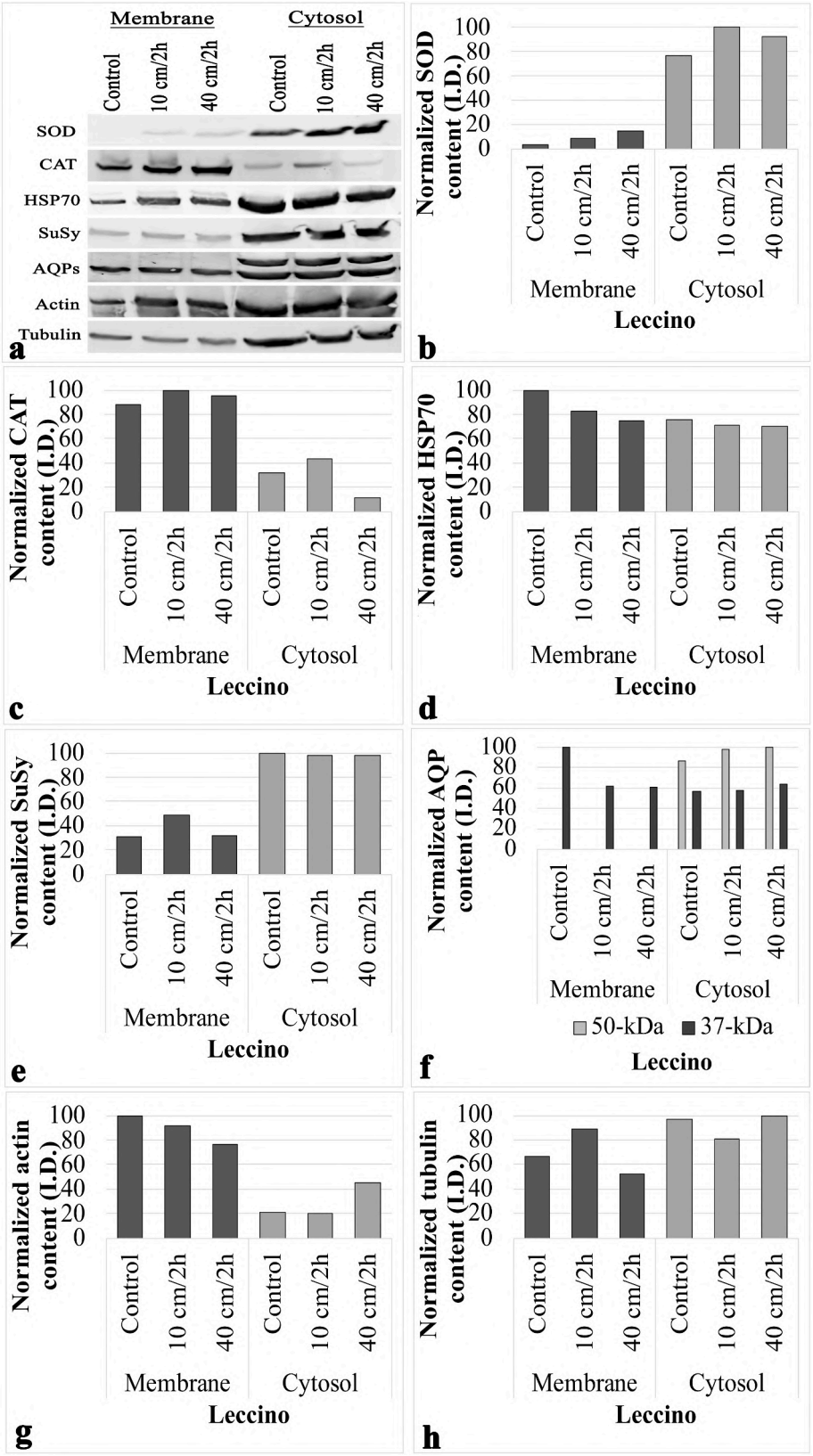


**Fig. 4.** The effect of UV-B radiation on protein contents in 'Leccino'. **a** Immunoblotting results for the seven analyzed proteins; **b** I.D. of the SOD bands; **c** I.D. of the CAT bands; **d** I.D. of the HSP70 bands; **e** I.D. of the SuSy bands; **f** I.D. of the AQPs bands; **g** I.D. of the actin bands; **h** I.D. of the tubulin bands. Both the raw immunoblotting data and the graphs of normalized data are related to protein samples extracted from membrane and cytosolic fractions under the following conditions: control, UV-B exposure at 10 cm/2 h and at 40 cm/2 h.

relatively uniform between the membrane and cytosolic fractions, whereas tubulin accumulated preferentially in the cytosolic fraction (Fig. 5a). To enable comparisons to be made between the two fractions and between the control and UVB-treated samples, the immunoblotting signals were normalized to the total protein content of each electrophoretic lane.

Following both treatments, SOD levels decreased in the membrane fraction but increased in the cytosolic fraction (Fig. 5b). CAT levels decreased in the UVB-treated membrane fractions, whereas a decrease was only observed in the 10 cm/2 h stressed cytosolic sample (see Fig. 5c). HSP70 levels increased in both the membrane and the cytosolic fractions following the treatments (Fig. 5d). SuSy levels in the membrane fraction increased slightly under both treatment conditions. In the cytosolic fraction, SuSy levels increased slightly after a 2 h UV-B exposure at 10 cm but decreased after a 1 h UV-B exposure at 40 cm (see Fig. 5e). An AQP immunoreactive band was detected at 37-kDa in 'Olivastra Seggianese'. The abundance of this band in the membrane fraction increased following both treatments. In the cytosolic fraction, AQP levels decreased following a 2 h UV-B exposure at 10 cm but remained unchanged after a 1 h UV-B exposure at 40 cm compared to the control (see Fig. 5f). In the membrane fraction, actin levels were similar to the control after a 2 h UV-B exposure at 10 cm but decreased following a 1 h UV-B exposure at 40 cm. Actin levels increased in cytosolic fractions following both treatments (Fig. 5g). In the membrane fraction, tubulin levels were comparable between the control and stressed samples. However, in the cytosolic fractions, tubulin levels decreased following both treatments (Fig. 5h).

Immunoblot analysis of protein extracts from the 'Pendolino' pollen membrane and cytosolic fractions (Fig. 6a) revealed that SOD levels were lower in the membrane fraction than in the cytosol. Conversely, CAT exhibited a stronger signal in the membrane fraction and a weaker signal in the cytosol. Both HSP70 and SuSy were present in both compartments, with slightly higher levels observed in the cytosol. The expression pattern of AQP was similar to that observed in 'Leccino'. A 37-kDa isoform was present in both the membrane and cytosolic fractions under all experimental conditions. In contrast, a 50-kDa isoform was only detected in the cytosol. The two cytoskeletal proteins, actin and tubulin, exhibited a comparable distribution between the membrane and cytosolic fractions. Although slight changes in protein content were observed, SOD levels were low in the membrane fraction. More distinct changes in SOD levels were observed in the cytosol: they increased after a 3 h UV-B exposure at 10 cm but decreased compared to the control after a 1 h UV-B exposure at 40 cm (Fig. 6b). Under both treatment conditions, CAT levels decreased in the membrane fraction but increased in the cytosolic fraction (Fig. 6c). Similarly, HSP70 levels increased in both the membrane and cytosolic fractions after treatment (Fig. 6d). SuSy levels in the membrane fraction increased after a 3 h UV-B exposure at 10 cm, but decreased compared to the control after a 1-h UV-B exposure at 40 cm. In the cytosolic fraction, SuSy levels increased under both treatment conditions (Fig. 6e). The level of 37-kDa AQP in the membrane fraction increased after 3 h of UV-B radiation at 10 cm, but decreased after 1 h of UV-B radiation at 40 cm. In the cytosolic fraction, the level of the 37-kDa AQP decreased following a 3-h UV-B exposure at 10 cm, but increased significantly after a 1 h UV-B exposure at 40 cm. The level of 50-kDa AQP in the cytosolic fraction was similar to the control level after a 3 h UV-B exposure at 10 cm but increased significantly after a 1 h UV-B exposure at 40 cm (Fig. 6f). Following a 3 h UV-B exposure at 10 cm, actin levels in the membrane fraction were similar to the control level; however, they decreased slightly following a 1 h UV-B exposure at 40 cm. In the cytosolic fraction, actin levels decreased slightly under both treatment conditions (see Fig. 6g). In the membrane fraction, tubulin levels increased following 3 h UV-B exposure at 10 cm; however, they decreased compared to the control group following 1 h UV-B exposure at 40 cm. However, in the cytosolic fraction, tubulin levels increased following both treatment conditions (Fig. 6h).

### 3.3. Integrated multivariate analysis

Heat-map analysis was used to compare the differences in various parameters between the control and stressed groups for all cultivars (Fig. 7). This multivariate approach integrates $R^2$ values derived from ROS distribution analyses with normalized percentage changes in biochemical and molecular parameters. This provides a quantitative framework for evaluating coordinated UV-B stress responses across cultivars, rather than relying on isolated variations in individual variables. In the heatmap, columns with the highest intensity of green indicate the groups with the greatest changes, while columns with the highest intensity of red indicate the groups with the least changes. In addition, a ranking was created by summing the total values of the cells in each column, as follows: 'Pendolino' 40 cm/1 h, 'Pendolino' 10 cm/3 h, 'Olivastra Seggianese' 40 cm/1 h, 'Olivastra Seggianese' 10 cm/2 h, 'Leccino' 10 cm/2h, and 'Leccino' 40 cm/2 h. Under UV-B exposure at 10 cm, the cultivars ranked from highest to lowest rate of change were: 'Pendolino' (10 cm/3 h), 'Olivastra Seggianese' (10 cm/2 h) and 'Leccino' (10 cm/2 h). Similarly, at 40 cm, the order was: 'Pendolino' (40 cm/1 h), 'Olivastra Seggianese' (40 cm/1 h) and 'Leccino' (40 cm/2 h). The clusterization was based on cultivar rather than exposure intensity. The high- and low-stressed 'Leccino' lay in one cluster, as did the 'Olivastra Seggiaanese' groups. 'Pendolino' 40 cm/1 h was grouped with 'Olivastra Seggianese' and showed more similarity in changes to it than to its high-stress relative. Finally, the measured parameters are heterogenically clustered allowing for experimental group-specific changes rather than changes based on biochemical function.

To further evaluate the coordinated behaviour of the measured indicators, a Pearson correlation analysis was performed across all treatment groups ($n = 6$). Only statistically significant correlations ($p < 0.05$) are reported in Supplementary File 1. The ROS distribution similarity showed a strong negative correlation with the total polyphenol content ($r = -0.87$). This indicates that treatments associated with higher phenolic accumulation tend to maintain more stable, tip-focused ROS gradients. A strong positive correlation was detected between the abundance of cytosolic catalase (CAT) and heat shock protein 70 (HSP70) ($r = 0.96$), suggesting the coordinated activation of antioxidant defence and protein-protection systems. Significant associations were also observed between membrane-associated antioxidant enzymes and structural components related to cytoskeletal organisation and water transport. These relationships reveal consistent patterns of parameter co-variation across treatments.

## 4. Discussion

This study combines biochemical data with existing evidence that UV-B primarily affects pollen tube cell wall architecture, resulting in cultivar-specific consequences for tip growth. From a mechanistic viewpoint, sustained pollen tube elongation requires (i) a spatially restricted ROS gradient at the apex that acts as a signalling module, (ii) efficient antioxidant buffering to prevent ROS diffusion causing global oxidative stress, (iii) cytoskeletal organisation to maintain polarised vesicle delivery and (iv) water influx through aquaporins to sustain turgor pressure and couple cell wall to growth. Therefore, UV-B tolerance can be interpreted as the capacity to preserve the coupling between redox homeostasis, turgor control and cell wall remodelling.

Excessive ROS accumulation caused by UV-B stress is known to damage biomolecules (Frohnmeyer and Staiger, 2003). In response, plants can boost their antioxidant systems, comprising both enzymatic (CAT and SOD) and non-enzymatic components (Frohnmeyer and Staiger, 2003; Rao et al., 2025). Murakami et al. (2004) found that chaperone proteins such as HSP70 can also mitigate ROS-induced damage. However, the disruption of ROS homeostasis can affect the mechanisms that control pollen tube elongation directly (Potocký et al., 2007). ROS could affect fundamental processes such as actin-directed exocytosis and turgor pressure either alone or in conjunction with

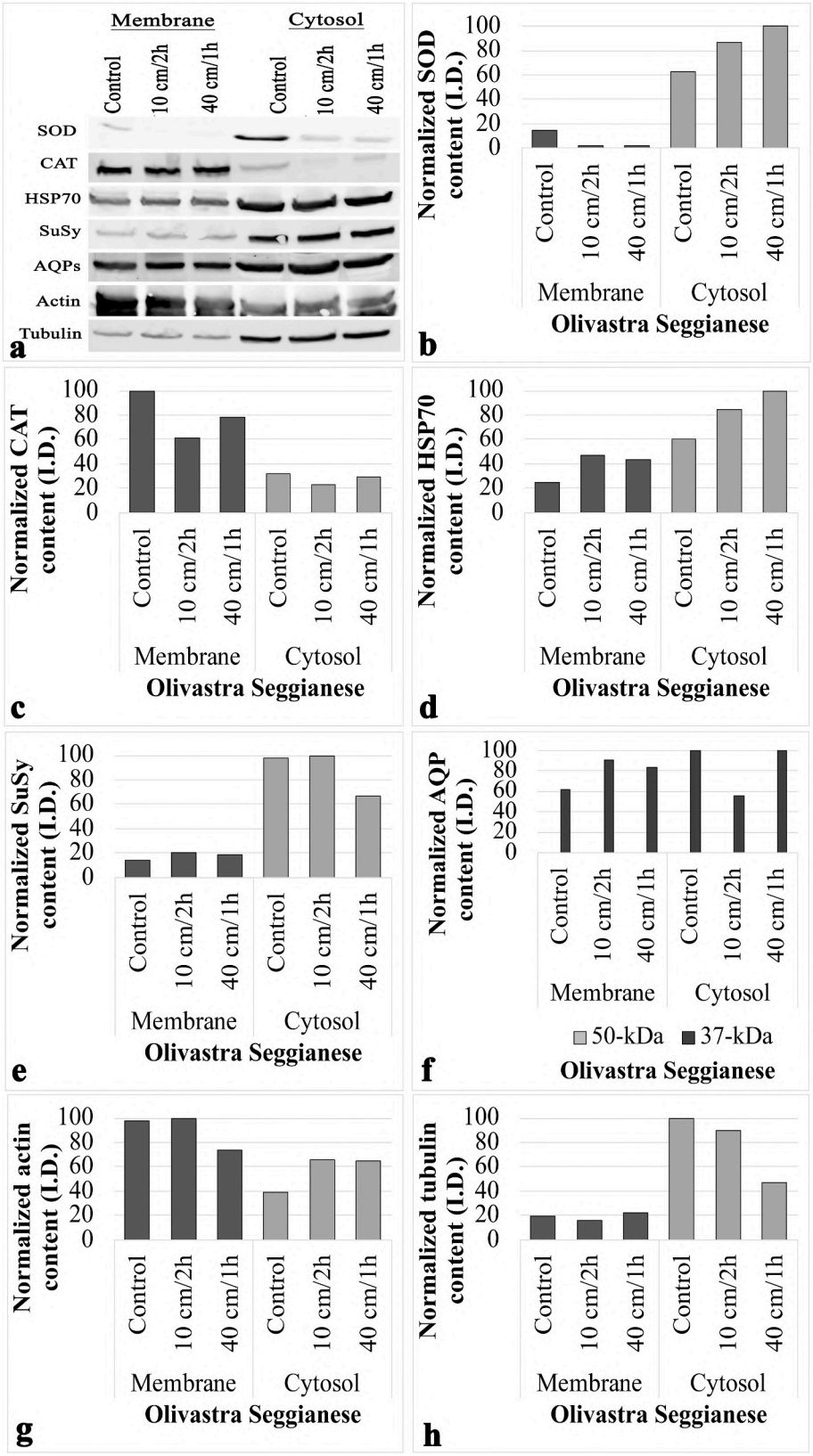


**Fig. 5.** The effect of UV-B radiation on protein contents in 'Olivastra Seggianese'. **a** Raw immunoblotting result of the analyzed proteins; **b** I.D. of the SOD bands; **c** I.D. of the CAT bands; **d** I.D. of the HSP70 bands; **e** I.D. of the SuSy bands; **f** I.D. of the AQPs bands; **g** I.D. of the actin bands; **h** I.D. of the tubulin bands. The raw immunoblotting and normalized data relate to protein samples extracted from membrane and cytosolic fractions under the following conditions: control; UV-B exposure at 10 cm for 2 h and at 40 cm for 1 h.

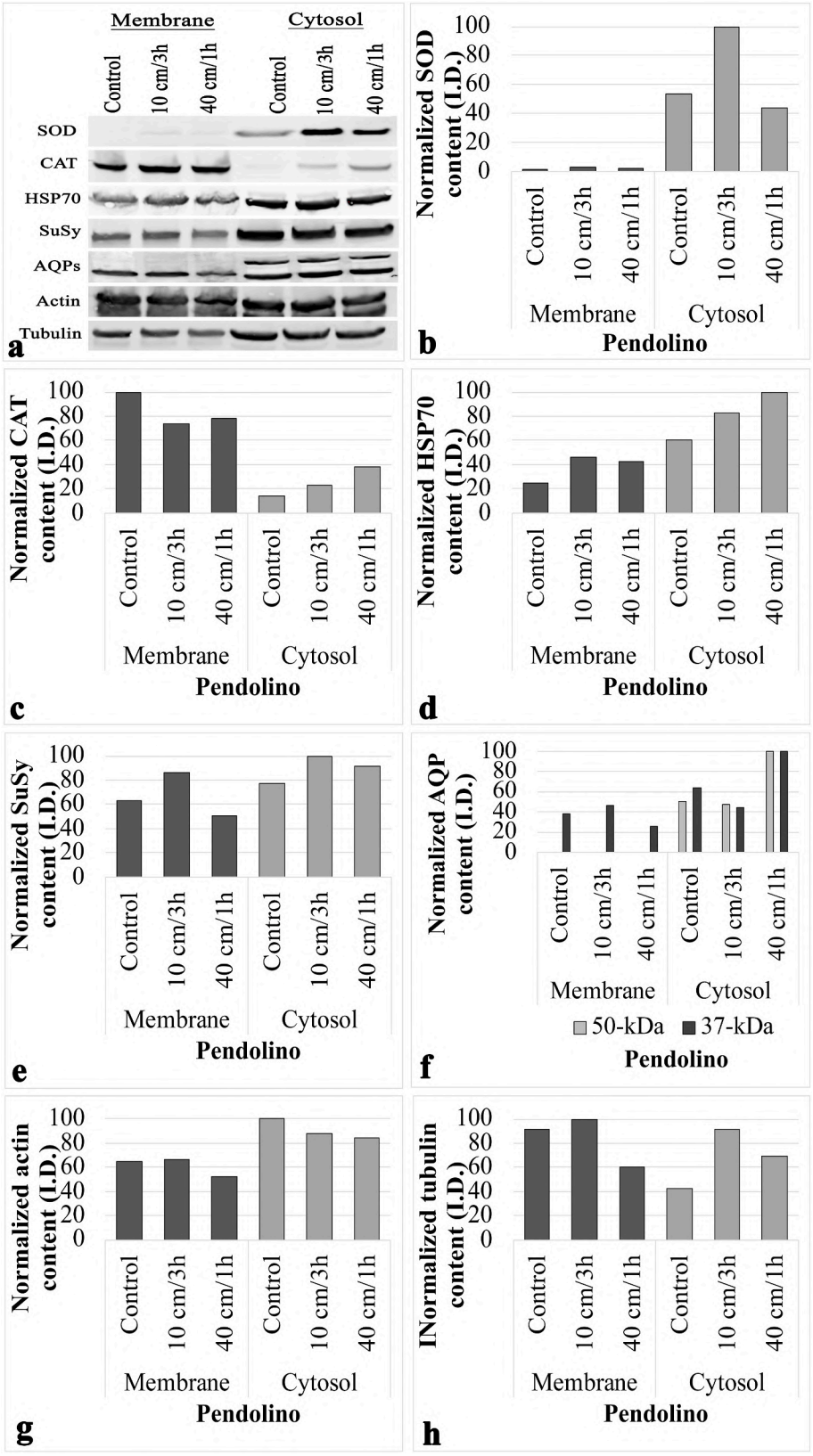


**Fig. 6.** The effect of UV-B radiation on protein contents in 'Pendolino'. **a** Immunoblotting results on the seven proteins analyzed; **b** I.D. of the SOD bands; **c** I.D. of the CAT bands; **d** I.D. of the HSP70 bands; **e** I.D. of the SuSy bands; **f** I.D. of the AQPs bands; **g** I.D. of the actin bands; **h** I.D. of the tubulin bands. The raw immunoblotting and normalized data relate to protein samples extracted from membrane and cytosolic fractions under the following conditions: control; UV-B exposure at 10 cm for 3 h and at 40 cm for 1 h.

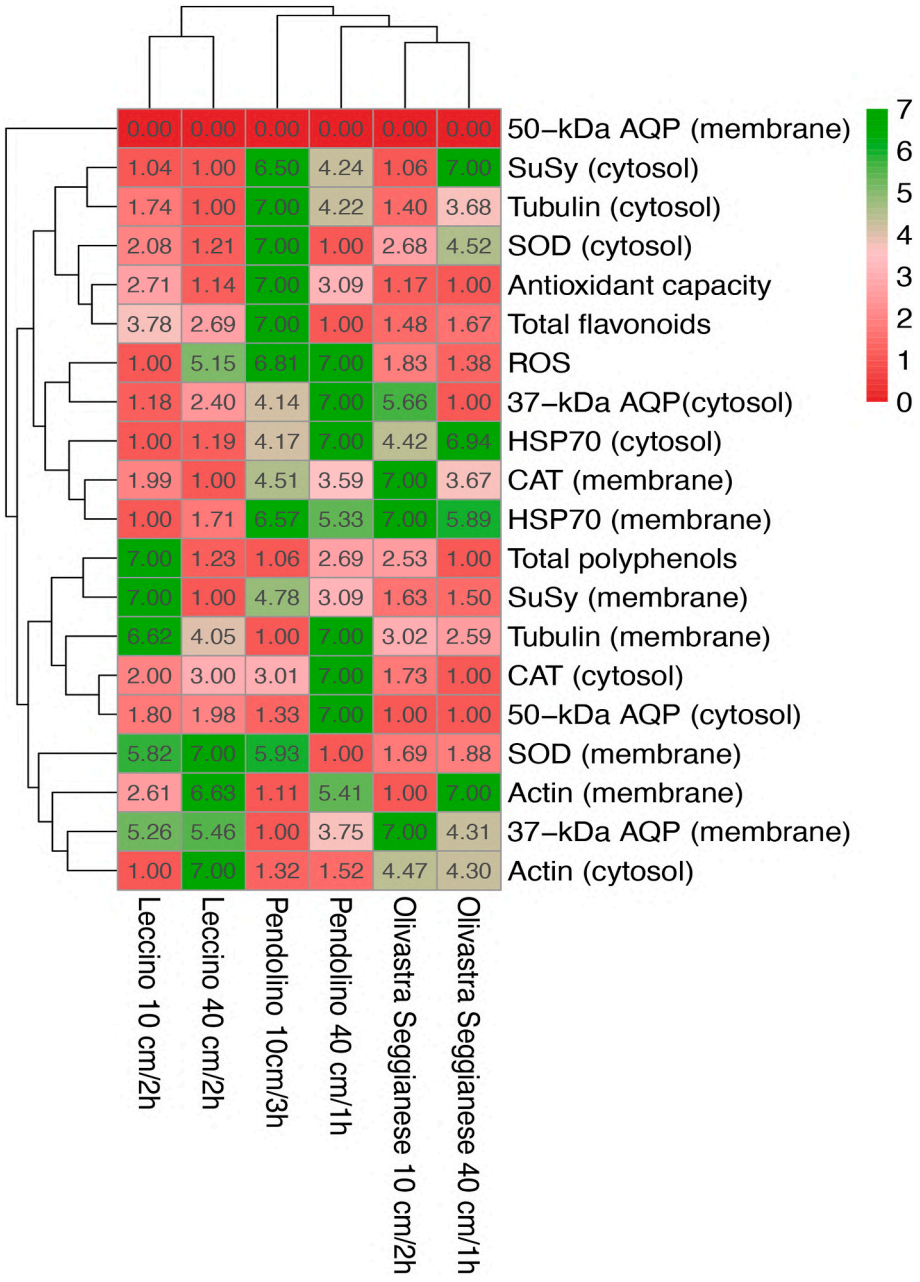


**Fig. 7.** Heat-map analysis of the UV-B stressed samples of all cultivars. The red color indicates low values, and the green color indicates high values.

$Ca^{2+}$ levels (Geitmann, 2010). Turgor is maintained by water uptake, facilitated by membrane-localized AQPs, particularly the 37-kDa AQP isoform (Wudick et al., 2014). Actin filaments promote vesicle trafficking and exocytosis of pectin-containing vesicles, while microtubules regulate the intracellular trafficking of cellulose synthase (CesA) and callose synthase (CalS). CesA and CalS are responsible for synthesizing cellulose and callose, respectively (Cai et al., 2011). These polysaccharides, together with acidic and esterified pectins, determine the mechanical properties of the cell wall, with SuSy playing a dual role. The membrane-bound form of SuSy provides the UDP-glucose necessary for cellulose and callose biosynthesis. Meanwhile, the cytosolic form of SuSy contributes to the metabolic energy balance, supporting both cell wall formation and cellular energy metabolism (Persia et al., 2008).

According to the heatmap analysis (Fig. 7), 'Leccino' and 'Olivastra Seggianese' exhibited lower coefficients of variation than 'Pendolino', which showed more pronounced fluctuations in several cellular parameters. This increased variability in 'Pendolino' likely reflects a reduced ability to stabilize ROS homeostasis, as indicated by elevated ROS levels, reduced membrane-associated CAT, and decreased AQP abundance. The stability of the other two cultivars corresponds with the consistent biochemical responses, such as the maintenance of AQP abundance and accumulation of enzymatic and non-enzymatic antioxidants. To gain a more comprehensive understanding of how olive pollen tubes respond to UV-B stress, we combined the biochemical findings from this study with the observations on cell walls reported in our previous work (Çetinbaş-Genç et al., 2024). The schematic diagrams in Fig. 8 summarise the structural and biochemical mechanisms involved in pollen tube elongation. The diagrams illustrate the significant variations in data from this study and summarise information from previous UV-B investigations (Çetinbaş-Genç et al., 2024). This integrated analysis reveals that differences between cultivars concern not only individual mechanisms, but also the coordination of redox homeostasis, turgor and cytoskeletal dynamics specific to each cultivar that support pollen tube growth.

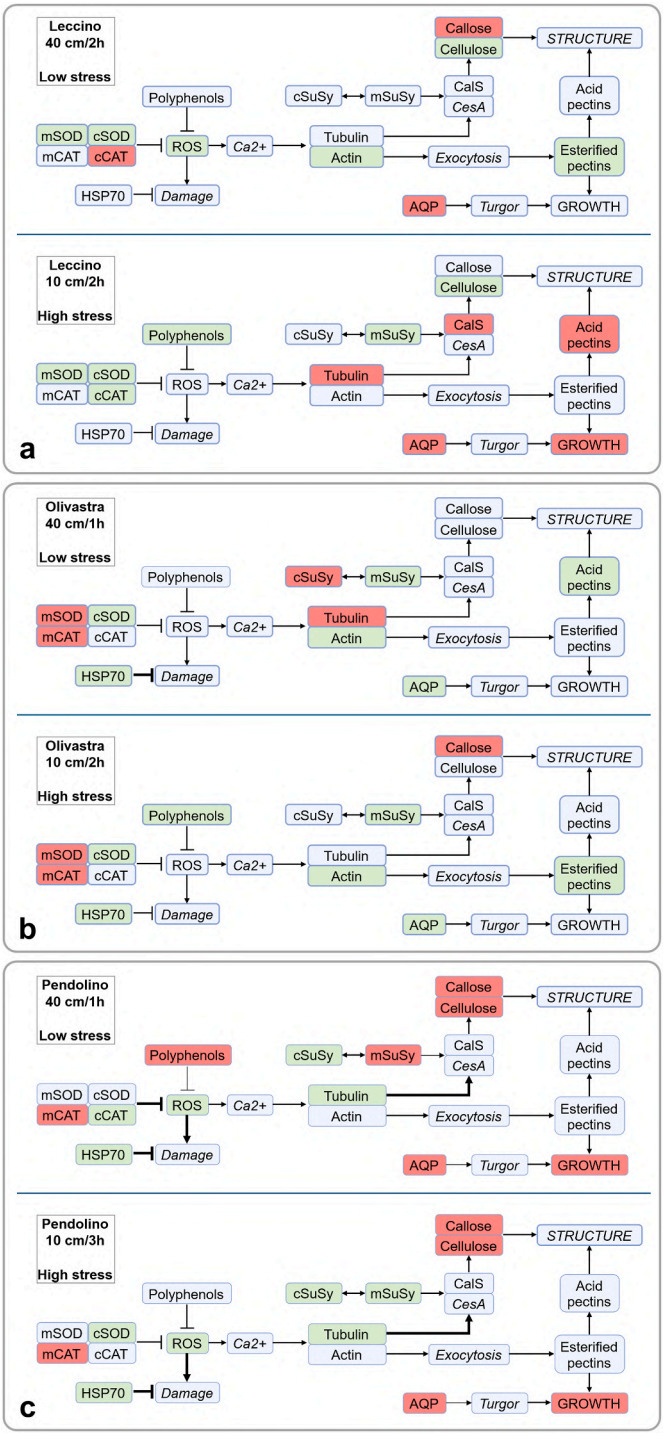


**Fig. 8.** Schematic representation of cultivar-specific responses. **a** 'Leccino', **b** 'Olivastra Seggianese', **c** 'Pendolino'. The red shapes show values in the treatment groups that are lower than those in the control group. The green shapes indicate higher values. Neutral colouring indicates a lack of variation. Parameters that are not measured directly are shown in italics. The arrows and T-end line indicate whether the biological process is enhanced or slowed down due to the measured parameter. Data on calcium (CalS), callose and cellulose accumulation, as well as on acid and esterified pectins and pollen tube growth, were obtained from Çetinbaş-Genç et al. (2024).

Even under high stress exposure (10 cm/2 h), 'Leccino' maintained a robust antioxidant pool, with unchanged HSP70 and increased polyphenol levels, thus keeping ROS at control-like levels. This is consistent with previous evidence suggesting that the accumulation of phenolic compounds in the tissues of *Silene littorea* acts as a protective mechanism against UV-B radiation (Del Valle et al., 2020). Phenolic compounds play a critical role in maintaining ROS homeostasis in pollen exposed to environmental stress (Xie et al., 2022). The observed association between increased polyphenol accumulation and maintenance of a tip-focused ROS distribution suggests that phenolic compounds play a protective role in stabilizing redox gradients under moderate UV-B exposure. Polyphenols are known to function as both efficient ROS scavengers and UV-absorbing molecules. This limits excessive oxidative stress while preserving the localised ROS signalling required for polarised pollen tube growth (Del Valle et al., 2020). In this context, the marked increase in total polyphenol content observed under the 10 cm/2 h UV-B exposure may help to stabilize ROS levels without disrupting the physiological ROS gradient at the pollen tube tip. This supports controlled growth under moderate UV-B stress. Despite ROS homeostasis being preserved in 'Leccino', our previous analysis revealed that high-stress treatment (10 cm/2 h) negatively impacted several cell wall components (Çetinbaş-Genç et al., 2024). Assuming that preserved ROS homeostasis maintains the stability of cytosolic $Ca^{2+}$ levels, cell wall modifications may be related to the observed decrease in tubulin, consistent with the high sensitivity of microtubules to UV-B radiation (Krasylenko et al., 2012). Together with reduced AQP levels, which are likely to disrupt turgor pressure, the negative effect of UV-B stress on the cell wall could explain the previously documented reduction in pollen tube growth (Çetinbaş-Genç et al., 2024). This is likely to disrupt turgor pressure. The negative effect of UV-B stress on the cell wall could explain the previously documented reduction in pollen tube growth (Çetinbaş-Genç et al., 2024). Under low stress conditions (40 cm/2 h), cell wall remodelling appears to be compensatory (Çetinbaş-Genç et al., 2024). Increased pectin deposition combined with decreased callose results in a less rigid cell wall structure, which may enable pollen tube growth despite the potential limitation of turgor associated with reduced AQPs. Although exocytosis was not measured here, an increase in actin levels could plausibly enhance the trafficking of vesicles to the apex and the subsequent deposition of esterified pectins (Fig. 8a). This interpretation is supported by evidence that actin filaments undergo structural reorganization in response to UV-B radiation (Chen and Han, 2016).

'Olivastra Seggianese' pollen tubes showed efficient and stable responses to cope with both low and high stress conditions. Given that ROS originate from the plasma membrane and organelles (Das and Roychoudhury, 2014), the decrease in membrane-localized SOD and CAT in both treatments suggests that 'Olivastra Seggianese' rapidly senses and effectively regulates UV-B stress. This cultivar also has higher basal polyphenols, even under control conditions, with a further increase only under high stress treatment (10 cm/2h), which mirrors UV-B-induced phenolic accumulation in leaves of *Brassica oleracea* (Yoon et al., 2022). Furthermore, it shows increased HSP70 under both treatments, resulting in ROS levels under both stress conditions comparable to those in the control group, likely supporting pollen tube growth. In parallel, maintenance of tube growth was presumably facilitated by the observed increase in actin, consistent with a role in maintaining both exocytosis and tip elongation; genes associated with actin organization are frequently upregulated in salt-tolerant *Arabidopsis* genotypes (Chun et al., 2021). The observed increase in HSP70 at both intensities may counteract ROS-induced protein damage, thereby indirectly promoting pollen tube growth. This finding is consistent with evidence that increased HSP70 expression improves tolerance to UV-B radiation (Murakami et al., 2004). As previously reported (Çetinbaş-Genç et al., 2024), the pollen of this cultivar exhibited a high pectin/callose ratio under UV-B; this, combined with a consistent AQP investment, indicates that the 'Olivastra Seggianese' pollen tube can adapt its structural components to maintain growth under stress. Notably, while the 37-kDa AQP band was present in all cultivars, a 50-kDa AQP band appeared in the cytosolic fractions of 'Leccino' and 'Pendolino' pollen tubes but was absent in 'Olivastra Seggianese' pollen tubes (Fig. 8b). This banding difference may be a cultivar-specific feature, consistent with reports

linking AQP isoform patterns to stress tolerance in tomato cultivars (Conti et al., 2022).

'Pendolino' showed more pronounced fluctuations in several cellular parameters (Figs. 7 and 8) compared to the other cultivars. Pollen tubes showed elevated ROS levels under both stress conditions. Since ROS are predominantly generated at membrane/organelle interfaces, membrane-localized antioxidant enzymes will provide a first line of defense (Sachdev et al., 2021). Here, membrane-associated SOD was unchanged in both treatments, while membrane CAT decreased, indicating a different antioxidant enzymatic pattern compared to 'Leccino' and 'Olivastra Seggianese'. Consistently, UV-B exposure did not significantly alter CAT/SOD activity in the leaves of the UV-B tolerant cultivar Giarraffa (Piccini et al., 2021), while distinct CAT/SOD responses were found in the less tolerant 'Olivastra Seggianese'. At lower stress (40 cm/1 h), 'Pendolino' uniquely showed reduced polyphenols and no increase in cytosolic SOD, suggesting ineffective activation by the stress signal, comparable to the dose-dependent ROS response (Ozgur et al., 2021). Our previous work (Çetinbaş-Genç et al., 2024) indicated that the cell wall integrity of the 'Pendolino' pollen tube was weakened by the low-stress treatment. The decrease in membrane-bound SuSy may have contributed to reduced cellulose and callose synthesis, resulting in a less stable cell wall architecture. In contrast, the increased cytosolic SuSy may imply a resource allocation towards energy conservation rather than cell wall biosynthesis suggesting that metabolic resources are not being allocated efficiently. Consequently, energy is conserved at the expense of cell wall biosynthesis. This imbalance helps to explain the wide variations that the 'Pendolino' shows across many cellular parameters. In fact, studies in maize, rice, and tobacco have shown that the distribution of SuSy in the cytoplasm or membrane can change significantly under stress (Mu et al., 2009; Li et al., 2022; Parrotta et al., 2016). The concomitant reduction of AQPs in the 'Pendolino' pollen tube under both stress conditions likely compromised turgor maintenance, consistent with the inhibition of pollen tube growth even at lower stress (40 cm/1 h). Increased HSP70 at low stress may indicate an effort to counteract ROS-induced protein damage and a repair-oriented rather than preventive approach when multiple structural defects are present (Fig. 8c). Finally, in 'Pendolino', the weak activation of both enzymatic and non-enzymatic antioxidants in response to UV-B radiation suggests that, while stress is detected, an effective, coordinated response is not initiated.

To complement the cultivar-specific comparisons, correlation analysis provided quantitative evidence of the coordinated regulation of redox balance, structural dynamics and stress-related proteins in response to UV-B exposure. While the limited number of treatment groups requires cautious interpretation, several significant associations were identified to reinforce the proposed mechanistic framework. Notably, the strong negative correlation between ROS distribution and total polyphenol content suggests that the accumulation of phenolic compounds contributes to the stabilisation of ROS gradients, thereby supporting polarised pollen tube growth. Similarly, the strong positive correlation between cytosolic CAT and HSP70 indicates the synchronised activation of antioxidant and protein folding protection systems, reflecting an integrated response to oxidative stress. It is important to note that these correlations were not intended to make direct comparisons between cultivars, but rather to identify general patterns of coordination among biochemical and structural parameters under UV-B stress. The quantitative relationships together support the concept that UV-B tolerance in olive pollen is not determined by the activation of isolated defence components, but rather by synchronised regulation of redox homeostasis, turgor control and cytoskeletal organisation.

The cultivar-dependent pollen responses observed in this study are of particular interest when considered alongside the well-documented ecological adaptation and stress tolerance profiles of Tuscan olive cultivars. Within this framework, 'Leccino' and 'Olivastra Seggianese' are generally recognized as having moderate to high tolerance of adverse environmental conditions, whereas 'Pendolino' is more sensitive, particularly at the reproductive level (Çetinbaş-Genç et al., 2024). Our results are consistent with these agronomic observations. 'Olivastra Seggianese', reported to exhibit high tolerance to adverse climatic conditions (Piccini et al., 2021), displayed the most stable and coordinated pollen response to UV-B radiation. This response was characterised by controlled ROS distribution, sustained antioxidant investment and preservation of cytoskeletal and water transport components. 'Leccino', which is known for its relatively good stress tolerance (Gucci et al., 2003), maintains redox homeostasis through enhanced antioxidant capacity. However, concomitant alterations in cytoskeletal elements and aquaporin abundance suggest that its tolerance strategy relies on partial compensation rather than full coordination. In contrast, Pendolino, generally considered less tolerant of environmental stress (Çetinbaş-Genç et al., 2024), exhibited pronounced variability and weak integration of redox regulation, turgor control and structural dynamics at the pollen level. Together, these observations suggest that pollen-level UV-B tolerance is indicative of broader, cultivar-specific adaptation patterns, and that reproductive resilience is likely to be determined by the ability to coordinate conserved cellular processes rather than by the activation of individual defence mechanisms alone. Consequently, the response patterns identified here could inform the evaluation of UV-B sensitivity in other olive cultivars and guide the selection of genotypes better suited to future Mediterranean environments characterised by increasing UV radiation.

## 5. Conclusion

This study, together with previous research (Çetinbaş-Genç et al., 2024), consistently demonstrates that the 'Pendolino' cultivar is more sensitive to low-intensity UV-B radiation. In contrast, the 'Leccino' and 'Olivastra Seggianese' cultivars exhibit a more balanced response under both high and low radiation intensities. Combined data provide mechanistic insights into the biochemical and molecular processes underlying these differences, showing that UV-B exposure induces distinct biochemical responses in olive pollen, which are cultivar-specific. While earlier work identified the pollen tube cell wall as the primary defense line and/or the initial target of UV-B-induced stress, current results reveal that UV-B-induced cell wall adjustments are accompanied by coordinated changes in both enzymatic and non-enzymatic antioxidant systems, as well as in proteins involved in cellular protection, metabolic regulation, and cytoskeletal dynamics. Taken together, these findings suggest that olive pollen from different cultivars employs distinct defense strategies to maintain pollen tube functionality under UV-B stress, and that tolerance to UV-B radiation varies between cultivars.

Beyond their mechanistic significance, these findings may have implications for cultivar selection in the context of future climate scenarios involving increased UV-B exposure. The coordinated biochemical and molecular responses observed in 'Olivastra Seggianese', such as stable ROS homeostasis, sustained antioxidant capacity and the maintenance of cytoskeletal and water transport components, suggest the presence of advantageous traits under elevated UV-B conditions. By contrast, the weaker integration of stress responses observed in 'Pendolino' suggests vulnerabilities that could restrict reproductive performance in such environments. Although the present study focuses on pollen-level responses, cultivar-specific tolerance patterns could inform breeding strategies aimed at improving reproductive resilience in the face of increasing UV-B stress.

## CRediT authorship contribution statement

Aslıhan Çetinbaş-Genç: Conceptualization, formal analysis, data curation, writing – original draft, writing – review and editing; Sara Parri: Conceptualization, formal analysis, data curation, writing – original draft, writing – review and editing; Silvia Licata: Formal analysis, data curation, software; Giampiero Cai: Conceptualization, formal analysis, data curation, writing – review and editing, supervision.

## Funding

This research did not receive any specific grant from funding agencies in the public, commercial, or not-for-profit sectors.

## Declaration of competing interest

The authors declare that they have no known competing financial interests or personal relationships that could have appeared to influence the work reported in this paper.

## Acknowledgments

We thank the 'The Scientific and Technological Research Council of Türkiye (TÜBİTAK)' for supporting the post-doctoral research grant of Aslıhan Çetinbaş Genç in the framework of '2219 - International Post-doctoral Research Fellowship Program for Turkish Citizens'. We also thank "National Research Council of Italy - Institute of BioEconomy (CNR-IBE) Santa Paolina Experimental Farm" (Follonica, Italy) for kindly providing the olive pollen used in the present work. We would also like to thank Dr Agata Di Noi, Dr Laura Giovanetti and Dr Tommaso Campani (Department of Physical, Earth and Environmental Sciences, University of Siena) for their valuable technical assistance with the use of the microplate reader.

## Appendix A. Supplementary data

Supplementary data to this article can be found online at https://doi.org/10.1016/j.plaphy.2026.111264.

## Data availability

Data will be made available on request.

## References

Allen Brady, G., Halloran, J.W., 1997. Stereolithography of ceramic suspensions. Rapid Prototyp. J. 3 (2), 61–65. https://doi.org/10.1108/13552549710176680.

Benzie, I.F., Strain, J.J., 1996. The ferric reducing ability of plasma (FRAP) as a measure of "antioxidant power": the FRAP assay. Anal. Biochem. 239 (1), 70–76. https://doi.org/10.1006/abio.1996.0292.

Brewbaker, J.L., Kwack, B.H., 1963. The essential role of calcium ion in pollen germination and pollen tube growth. Am. J. Bot. 50 (9), 859–865. https://doi.org/10.2307/2439772.

Cai, G., Faleri, C., Del Casino, C., Emons, A.M.C., Cresti, M., 2011. Distribution of callose synthase, cellulose synthase, and sucrose synthase in tobacco pollen tube is controlled in dissimilar ways by actin filaments and microtubules. Plant Physiol. 155 (3), 1169–1190. https://doi.org/10.1104/pp.110.171371.

Cascallares, M., Setzes, N., Marchett, F., López, G.A., Dstéfano, A.M., Canzos, M., Zabeleta, E., Pagnussat, G.C., 2020. A complex journey: cell wall remodeling, interactions and integrity during pollen tube growth. Front. Plant Sci. 11, 599247. https://doi.org/10.3389/fpls.2020.599247.

Çetinbaş-Genç, A., Faleri, C., Parri, S., Cantini, C., 2024. Differential responses of the pollen tube cell wall of Italian olive cultivars to UV-B radiation. Plant Stress 15 (5), 100734. https://doi.org/10.1016/j.stress.2024.100734.

Chebli, Y., Geitmann, A., 2007. Mechanical principles governing pollen tube growth. Funct. Plant Sci. Biotechnol. 1 (2), 232–245.

Chen, H., Han, R., 2016. Characterization of actin filament dynamics during mitosis in wheat protoplasts under UV-B radiation. Sci. Rep. 6 (1), 20115. https://doi.org/10.1038/srep20115.

Chun, H.J., Lim, L.H., Cheong, M.S., Baek, D., Park, M.S., Cho, H.M., Lee, S.H., Byung Jun Jin, B.J., No, D.H., Cha, Y.J., Lee, Y.B., Hong, J.C., Yun, D.J., Kim, M.C., 2021. Arabidopsis CCoAOMT1 plays a role in drought stress response via ROS-and ABA-dependent manners. Plants 10 (5), 831. https://doi.org/10.3390/plants10050831.

Conti, V., Cantini, C., Romi, M., Cesare, M.M., Parrotta, L., Del Duca, S., Cai, G., 2022. Distinct tomato cultivars are characterized by a differential pattern of biochemical responses to drought stress. Int. J. Mol. Sci. 23 (10), 5412. https://doi.org/10.3390/ijms23105412.

Cun, S., Zhang, C., Chen, J., Qian, L., Sun, H., Song, B., 2024. Effects of UV-B radiation on pollen germination and tube growth: a global meta-analysis. Sci. Total Environ. 915, 170097. https://doi.org/10.1016/j.scitotenv.2024.170097.

Das, K., Roychoudhury, A., 2014. Reactive oxygen species (ROS) and response of antioxidants as ROS-scavengers during environmental stress in plants. Front. Environ. Sci. 2, 53. https://doi.org/10.3389/fenvs.2014.00053.

Del Casino, C., Conti, V., Licata, S., Cai, G., Cantore, A., Ricci, C., Cantara, S., 2024. Mitigation of UV-B radiation stress in tobacco pollen by expression of the tardigrade damage suppressor protein (Dsup). Cells 13 (10), 840. https://doi.org/10.3390/cells13100840.

Del Valle, J.C., Buide, M.L., Whittall, J.B., Valladares, F., Narbona, E., 2020. UV radiation increases phenolic compound protection but decreases reproduction in *Silene littorea*. PLoS One 15 (6), e0231611. https://doi.org/10.1371/journal.pone.0231611.

Du, M.T., Zhu, G.L., Chen, H.Z., Han, R., 2021. Actin filaments altered distribution in wheat (*Triticum aestivum*) "Bending Root" to respond to enhanced Ultraviolet-B radiation. Braz. J. Biol. 81, 684–691. https://doi.org/10.1590/1519-6984.229774.

Frohnmeyer, H., Staiger, D., 2003. Ultraviolet-B radiation-mediated responses in plants. Balancing damage and protection. Plant Physiol. 133 (4), 1420–1428. https://doi.org/10.1104/pp.103.030049.

Fujita, M., Hasanuzzaman, M., 2022. Approaches to enhancing antioxidant defense in plants. Antioxidants 11 (5), 925. https://doi.org/10.3390/antiox11050925.

Galili, T., O'Callaghan, A., Sidi, J., Sievert, C., 2018. Heatmaply: an R package for creating interactive cluster heatmaps for online publishing. Bioinformatics 34 (9), 1600–1602. https://doi.org/10.1093/bioinformatics/btx657.

Geitmann, A., 2010. How to shape a cylinder: pollen tube as a model system for the generation of complex cellular geometry. Sex. Plant Reprod. 23 (1), 63–71. https://doi.org/10.1007/s00497-009-0121-4.

Gucci, R., Servili, M., Esposto, S., Selvaggini, R., 2003. Oil quality of olive cv.'Leccino' grown under irrigated or dryfarmed conditions. IV International Symposium on Irrigation of Horticultural Crops 664, 297–302. https://doi.org/10.17660/ActaHortic.2004.664.36.

Hepler, P.K., Rounds, C.M., Winship, L.J., 2013. Control of cell wall extensibility during pollen tube growth. Mol. Plant 6 (4), 998–1017. https://doi.org/10.1093/mp/sst103.

Iwabuchi, K., Hidema, J., Tamura, K., Takagi, S., Hara-Nishimura, I., 2016. Plant nuclei move to escape ultraviolet-induced DNA damage and cell death. Plant Physiol. 170 (2), 678–685. https://doi.org/10.1104/pp.15.01400.

Kasthurirengan, S., Hong, Y., Ramachandran, S., 2025. Assessing Jatropha curcas pollen viability: a comparative assessment of transgenic and non-transgenic pollen under various environmental conditions using rapid staining technique. Front. Plant Sci. 16, 1543947. https://doi.org/10.3389/fpls.2025.1543947.

Kaya, H., Nakajima, R., Iwano, M., Kanaoka, M.M., Kimura, S., Takeda, S., Kawarazaki, T., Senzaki, E., Hamamura, Y., Higashiyama, T., Machida, Y., 2014. Ca2+-Activated reactive oxygen species production by arabidopsis RbohH and RbohJ is essential for proper pollen tube tip growth. Plant Cell 26 (3), 1069–1080. https://doi.org/10.1105/tpc.113.120642.

Khaerani, P.I., Musa, Y., Anichini, S., Parri, S., Faleri, C., Cai, G., 2025. Effect of UV-B stress on olive (*Olea europaea* L.) pollen tubes: a study of callose plug deposition and male germ unit integrity. Protoplasma 262 (3), 475–487. https://doi.org/10.1007/s00709-024-02010-4.

Koubouris, G.C., Metzidakis, I.T., Vasilakakis, M.D., 2009. Impact of temperature on olive (*Olea europaea* L.) pollen performance in relation to relative humidity and genotype. Environ. Exp. Bot. 67 (1), 209–214. https://doi.org/10.1016/j.envexpbot.2009.06.002.

Krasylenko, Y.A., Yemets, A.I., Sheremet, Y.A., Blume, Y.B., 2012. Nitric oxide as a critical factor for perception of UV-B irradiation by microtubules in Arabidopsis. Physiol. Plantarum 145 (4), 505–515. https://doi.org/10.1111/j.1399-3054.2011.01530.x.

Krasylenko, Y.A., Yemets, A.I., Blume, Y.B., 2013. Plant microtubules reorganization under the indirect UV-B exposure and during UV-B-induced programmed cell death. Plant Signal. Behav. 8 (5), e24031. https://doi.org/10.4161/psb.24031.

Kravets, E.A., Plokhovska, S.G., Yemets, A.I., Blume, Y.B., 2023. UV-B stress and plant sexual reproduction. In: UV-B Radiation and Crop Growth. Springer Nature Singapore, pp. 293–317. https://doi.org/10.1007/978-981-19-3620-3_14.

Lei, L., Li, S., Gu, Y., 2012. Cellulose synthase complexes: composition and regulation. Front. Plant Sci. 3, 75. https://doi.org/10.3389/fpls.2012.00075.

Li, H., Tiwari, M., Tang, Y., Wang, L., Yang, S., Long, H., Guo, J., Wang, Y., Wang, H., Yang, Q., Jagadish, S.V.K., Shao, R., 2022. Metabolomic and transcriptomic analyses reveal that sucrose synthase regulates maize pollen viability under heat and drought stress. Ecotoxicol. Environ. Saf. 246, 114191. https://doi.org/10.1016/j.ecoenv.2022.114191.

Mahdavian, K., 2024. Effects of ultraviolet radiation on plants and their protective mechanisms. Russ. J. Plant Physiol. 71 (6), 184. https://doi.org/10.1134/S1021443724607481.

Martin, R.E., Postiglione, A.E., Muday, G.K., 2022. Reactive oxygen species function as signaling molecules in controlling plant development and hormonal responses. Curr. Opin. Plant Biol. 69, 102293. https://doi.org/10.1016/j.pbi.2022.102293.

Mu, H., Ke, J., Liu, W., Zhuang, C., Yip, W., 2009. UDP-glucose pyrophosphorylase2 (OsUgp2), a pollen-preferential gene in rice, plays a critical role in starch accumulation during pollen maturation. Chin. Sci. Bull. 54 (2), 234–243. https://doi.org/10.1007/s11434-008-0568-y.

Muhlemann, J.K., Younts, T.L.B., Muday, G.K., 2018. Flavonols control pollen tube growth and integrity by regulating ROS homeostasis during high-temperature stress. Proc. Natl. Acad. Sci. USA 115 (47), E11188–E11197. https://doi.org/10.1073/pnas.1811492115.

Mukhopadhyay, R., Boro, P., Karmakar, K., Pradhan, P., Saha Chowdhury, R., Das, B., Mandan, R., Kumar, D., 2024. Advances in the understanding of heat shock proteins and their functions in reducing abiotic stress in plants. JPBB 1–18. https://doi.org/10.1007/s13562-024-00895-z.

Murakami, M., Yamaguchi, T., Takamura, H., Atoba, T.M., 2004. Effects of thermal treatment on radical-scavenging activity of single and mixed polyphenolic

compounds. J. Food Sci. 69 (1), FCT7–FCT10. https://doi.org/10.1111/j.1365-2621.2004.tb17848.x.
Ozgur, R., Uzilday, B., Yalcinkaya, T., Akyol, T.Y., Yildirim, H., Turkan, I., 2021. Differential responses of the scavenging systems for reactive oxygen species (ROS) and reactive carbonyl species (RCS) to UV-B irradiation in Arabidopsis thaliana and its high altitude perennial relative Arabis alpina. Photochem. Photobiol. Sci. 20 (7), 889–901. https://doi.org/10.1007/s43630-021-00067-1.
Pan, X., Zheng, Y., Lei, K., Tao, W., Zhou, N., 2024. Systematic analysis of heat shock protein 70 (HSP70) gene family in radish and potential roles in stress tolerance. BMC Plant Biol. 24 (1), 2. https://doi.org/10.1186/s12870-023-04653-6.
Parrotta, L., Cresti, M., Cai, G., 2013. Heat-shock protein 70 binds microtubules and interacts with kinesin in tobacco pollen tubes. Cytoskeleton 70 (9), 522–537. https://doi.org/10.1002/cm.21134.
Parrotta, L., Faleri, C., Cresti, M., Cai, G., 2016. Heat stress affects the cytoskeleton and the delivery of sucrose synthase in tobacco pollen tubes. Planta 243 (1), 43–63. https://doi.org/10.1007/s00425-015-2394-1.
Pérez Di Giorgio, J.A., Barberini, M.L., Amodeo, G., Muschietti, J.P., 2017. Pollen aquaporins: what are they there for? Plant Signal. Behav. 11 (9), e1217375. https://doi.org/10.1080/15592324.2016.1217375.
Persia, D., Cai, G., Del Casino, C., Faleri, C., Willemse, M.T., Cresti, M., 2008. Sucrose synthase is associated with the cell wall of tobacco pollen tubes. Plant Physiol. 147 (4), 1603–1618. https://doi.org/10.1104/pp.108.115956.
Piccini, C., Cai, G., Dias, M.C., Araújo, M., Parri, S., Romi, M., Faleri, C., Cantini, C., 2021. Olive varieties under UV-B stress show distinct responses in terms of antioxidant machinery and isoform/activity of RubisCO. Int. J. Mol. Sci. 22 (20), 11214. https://doi.org/10.3390/ijms222011214.
Podobedova, A., Baranova, E.N., Gulevich, A.A., Chaban, I.A., Breygina, M., 2025. Comprehensive study of sexual reproduction in *Nicotiana tabacum* plants overexpressing H2O2-Producing enzymes: superoxide dismutase and choline oxidase. Plants 14 (14), 2103. https://doi.org/10.3390/plants14142103.
Podolyan, A., Luneva, O.G., Klimenko, E.S., Breygina, M.A., 2021. Oxygen radicals and cytoplasm zoning in growing lily pollen tubes. Plant Reprod. 34 (2), 1–13. https://doi.org/10.1007/s00497-021-00403-6.
Potocký, M., Jones, M.A., Bezvoda, R., Smirnoff, N., Žárský, V., 2007. Reactive oxygen species produced by NADPH oxidase are involved in pollen tube growth. New Phytol. 174 (4), 742–751. https://doi.org/10.1111/j.1469-8137.2007.02042.x.
Rao, M.J., Duan, M., Zhou, C., Jiao, J., Cheng, P., Yang, L., Wei, W., Shen, Q., Ji, P., Zheng, B., 2025. Antioxidant defense system in plants: reactive oxygen species production, signaling, and scavenging during abiotic stress-induced oxidative damage. Horticulturae 11 (5), 477. https://doi.org/10.3390/horticulturae11050477.
Ren, R., Jiang, X., Di, W., Li, Z., Li, B., Xu, J., Liu, Y., 2019. HSP70 improves the viability of cryopreserved Paeonia lactiflora pollen by regulating oxidative stress and apoptosis-like programmed cell death events. PCTOC 139 (1), 53–64. https://doi.org/10.1007/s11240-019-01661-z.
Sachdev, S., Ansari, S.A., Ansari, M.I., Fujita, M., Hasanuzzaman, M., 2021. Abiotic stress and reactive oxygen species: generation, signaling, and defense mechanisms. Antioxidants 10 (2), 277. https://doi.org/10.3390/antiox10020277.
Salnikov, V.V., Grimson, M.J., Delmer, D.P., Haigler, C.H., 2001. Sucrose synthase localizes to cellulose synthesis sites in tracheary elements. Phytochemistry (Elsevier) 57 (6), 823–833. https://doi.org/10.1016/S0031-9422(01)00045-0.
Serrazina, S., Dias, F.V., Malhó, R., 2014. Characterization of FAB 1 phosphatidylinositol kinases in A rabidopsis pollen tube growth and fertilization. New Phytol. 203 (3), 784–793. https://doi.org/10.1111/nph.12836.
Shahzaidi, Z.S., Tackallou, S.H., Amjad, L., Zali, H., Iranbakhsh, A., 2025. Analysis of UV radiation-induced changes: effects on morpho-physiological, and biochemical traits of Portulaca oleracea. BMC Plant Biol. 25 (1), 1318. https://doi.org/10.1186/s12870-025-07386-w.
Sharma, S., Chatterjee, S., Kataria, S., Joshi, J., Datta, S., Vairale, M.G., Veer, V., 2017. A Review on Responses of Plants to UV-B Radiation Related Stress, vols. 75–97. UV-B Radiation: From Environmental Stressor to Regulator of Plant Growth. https://doi.org/10.1002/9781119143611.ch5.
Shi, C., Liu, H., 2021. How plants protect themselves from ultraviolet-B radiation stress. Plant Physiol. 187 (3), 1096–1103. https://doi.org/10.1093/plphys/kiab245.
Singleton, V.L., Rossi, J.A., 1965. Colorimetry of total phenolics with phosphomolybdic-phosphotungstic acid reagents. Am. J. Enol. Vitic. 16 (3), 144–158. https://doi.org/10.5344/ajev.1965.16.3.144.
Smirnova, L.P., Pervykh, L.N., 1998. Quantitative determination of the total content of flavonoids in the flowers of immortelle *Helichrysum arenarium*. Pharm. Chem. J. 32 (6), 321–324. https://doi.org/10.1007/BF02580519.
Sommer, A., Geist, B., Da Ines, O., Gehwolf, R., Schäffner, A.R., Obermeyer, G., 2008. Ectopic expression of *Arabidopsis thaliana* plasma membrane intrinsic protein 2 aquaporins in lily pollen increases the plasma membrane water permeability of grain but not of tube protoplasts. New Phytol. 180, 787–797. https://doi.org/10.1111/j.1469-8137.2008.02607.x.
Tan, S., Sha, Y., Sun, L., Li, Z., 2023. Abiotic stress-induced leaf senescence: regulatory mechanisms and application. Int. J. Mol. Sci. 24 (15), 11996. https://doi.org/10.3390/ijms241511996.
Ulm, R., Jenkins, G.I., 2015. Q&A: how do plants sense and respond to UV-B radiation? BMC Biol. 13 (1), 45. https://doi.org/10.1186/s12915-015-0156-y.
Wang, W., Sheng, X., Shu, Z., Li, D., Pan, J., Ye, X., Chang, P., Li, X., Wang, Y., 2016. Combined cytological and transcriptomic analysis reveals a nitric oxide signaling pathway involved in cold-inhibited *Camellia sinensis* pollen tube growth. Front. Plant Sci. 7, 456. https://doi.org/10.3389/fpls.2016.00456.
Winter, H., Huber, J.L., Huber, S.C., 1998. Identification of sucrose synthase as an actin-binding protein. FEBS (Fed. Eur. Biochem. Soc.) Lett. 430 (3), 205–208. https://doi.org/10.1016/S0014-5793(98)00659-0.
Wudick, M.M., Luu, D.T., Tournaire-Roux, C., Sakamoto, W., Maurel, C., 2014. Vegetative and sperm cell-specific aquaporins of Arabidopsis highlight the vacuolar equipment of pollen and contribute to plant reproduction. Plant Physiol. 164 (4), 1697–1706. https://doi.org/10.1104/pp.113.228700.
Xie, D.L., Zheng, X.L., Zhou, C.Y., Kanwar, M.K., Zhou, J., 2022. Functions of redox signaling in pollen development and stress response. Antioxidants 11 (2), 287. https://doi.org/10.3390/antiox11020287.
Yoon, H.I., Kim, J., Oh, M.M., Son, J.E., 2022. Prediction of phenolic contents based on ultraviolet-b radiation in three-dimensional structure of kale leaves. Front. Plant Sci. 13, 918170. https://doi.org/10.3389/fpls.2022.918170.
Zeng, Y., Guo, C., Wang, M., Jin, J., Yu, K., Zhang, J., Cao, F., 2024. Comprehensive evaluation of drought tolerance of six Chinese chestnut varieties (clones) based on flavonoids and other physiological indexes. Sci. Rep. 14 (1), 14511. https://doi.org/10.1038/s41598-024-65479-2.
Zhang, Y.C., He, R.R., Lian, J.P., Zhou, Y.F., Zhang, F., Li, Q.F., Yu, Y., Feng, Y.Z., Yang, Y.W., Lei, M.Q., He, H., Zhang, Z., Chen, Y.Q., 2020. OsmiR528 regulates rice-pollen intine formation by targeting an uclacyanin to influence flavonoid metabolism. Proc. Natl. Acad. Sci. USA 117 (1), 727–732. https://doi.org/10.1073/pnas.1810968117.
Zhao, C., Siddique, A.B., Guo, C., Shabala, S., Li, C., Chen, Z., Varshney, R., Zhou, M., 2025. A high-throughput protocol for testing heat-stress tolerance in pollen. aBIOTECH 6 (1), 63–71. https://doi.org/10.1007/s42994-024-00183-3.